Electronic supplementary information (ESI)

Real-Time Observation of Molecular Flattening and Intersystem Crossing in [(DPEPhos)Cu(I)(PyrTet)] *via* Ultrafast UV/Vis- and mid-IR Spectroscopy on Solution and Solid Samples

Merten Grupe,[a] Florian Bäppler,[a] Maximilian Theiß,[a] Jasmin M. Busch,[c] Fabian Dietrich,[b†] Daniel Volz,[c] Markus Gerhards,[b] Stefan Bräse[c,d] and Rolf Diller*[a]

[a] Physics Department, TU Kaiserslautern, Erwin-Schrödinger-Straße 46, 67663 Kaiserslautern, Germany. E-mail: diller@physik.uni-kl.de; Tel: +49 631 2052323

[b] Chemistry Department and Research Center Optimas, TU Kaiserslautern, Erwin-Schrödinger-Straße 52, 67663 Kaiserslautern, Germany

[c] Institute of Organic Chemistry, Karlsruhe Institute of Technology, Fritz-Haber-Weg 6, 76131 Karlsruhe, Germany

[d] Institute of Biological and Chemical Systems - Functional Molecular Systems, IBCS - FMS, Karlsruhe Institute of Technology, Hermann-von-Helmholtz-Platz 1, D-76344 Eggenstein-Leopoldshafen, Germany

[†] Present address: Núcleo Milenio MultiMat & Physics Department, Universidad de La Frontera, Francisco Salazar 01145, Temuco, Chile

***Corresponding Authors**

E-mail: diller@physik.uni-kl.de; Fax: +49 631 205-3902; Phone: +49 631 205-2323,

Figures:

Static spectra:

Time resolved spectra:

TD-DFT (B3LYP/def2-TZVP) results:

Sample integrity:

Tables:

Static spectra:

Static UV/Vis spectra of 1 in DCM, ACN, THF, DMSO, EtOH.

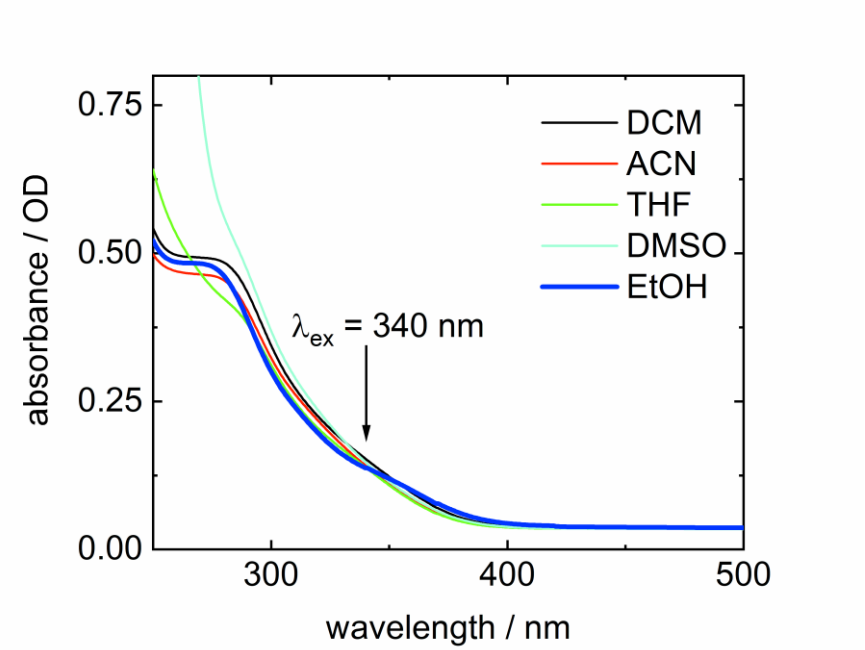

Figure S1. Ground state absorbance spectra of **1** dissolved in DCM (c = 0.021 mmol L^{-1}), ACN (c = 0.016 mmol L^{-1}), THF (c = 0.016 mmol L^{-1}), DMSO (c = 0.017 mmol L^{-1}) and EtOH (c = 0.020 mmol L^{-1}).

Table S1. The decadic extinction coefficient ε of 1 at 340 nm in various solvents as determined *via* absorbance measurement at given concentration.

Solvent	**ε at 340 nm** / 10^4 M^{-1} cm^{-1}
ACN	0.66 ± 0.13
DMSO	0.61 ± 0.03
THF	0.64 ± 0.03
EtOH	0.48 ± 0.03
DCM	0.58 ± 0.03

Table S2. Viscosity, dipole moment and relative permittivity of the used solvents.

Solvent	**Viscosity**[1] /mPa s at 25 °C	**Dipolemoment**[1] /Debye	**Rel. permittivity**[1]
DCM	0.413	1.60	8.93 (25 °C)
EtOH	1.074	1.69	25.3 (20 °C)
DMSO	1.987	3.96	47.24 (20 °C)
ACN	0.334	3.92	36.64 (20 °C)
THF	0.456	1.75	7.52 (22 °C)

Mid-IR ground state spectra.

Figure 1b (main text) and Figure S2 show the mid-IR absorption spectra of **1** in DCM-D_2 and as neat powder, respectively. Overall, they are very similar, suggesting correspondingly similar molecular structure in solution and as solid. However, below 1200 cm^{-1}, in solution relatively unstructured and broad absorbance features are in contrast to rather structured and narrow bands in the solid, suggesting strong dynamic interaction of solvent molecules with H-rocking and -scissoring vibrations in this region.

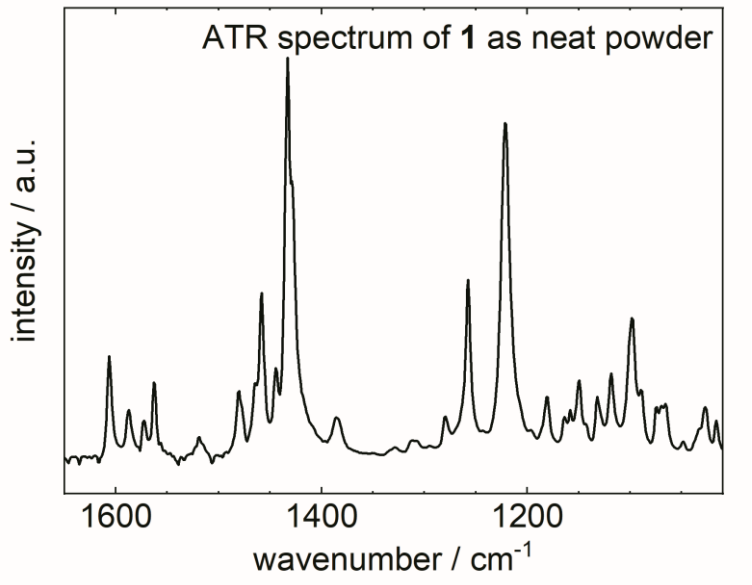

Figure S2. ATR-IR electronic ground state spectrum of **1** as neat powder.

2D static luminescence excitation spectra of 1 in ACN, DMSO, EtOH, DCM, THF, as neat and PMMA film.

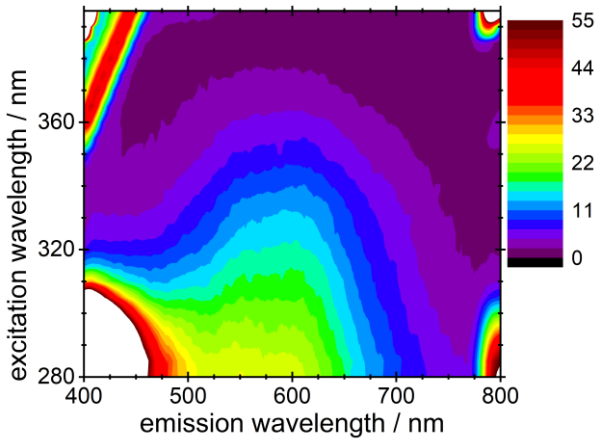

Figure S3. Static 2D luminescence excitation spectrum of **1** in ACN with OD = 0.12 (1 cm path) at 340 nm (ignore (scattering) artifacts in corners).

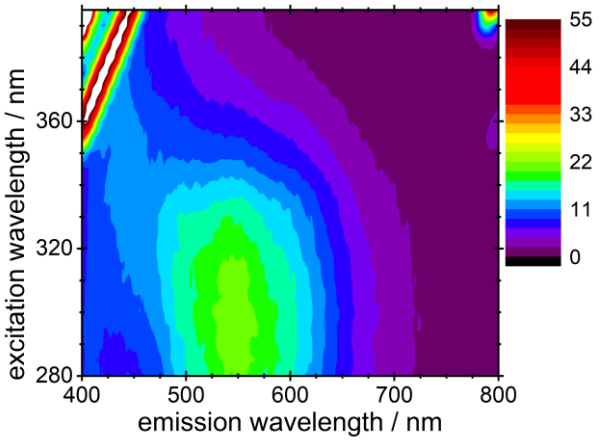

Figure S4. Static 2D luminescence excitation spectrum of **1** in DMSO with OD = 0.15 (1 cm path) at 340 nm (ignore scattering artifacts in upper left/right part).

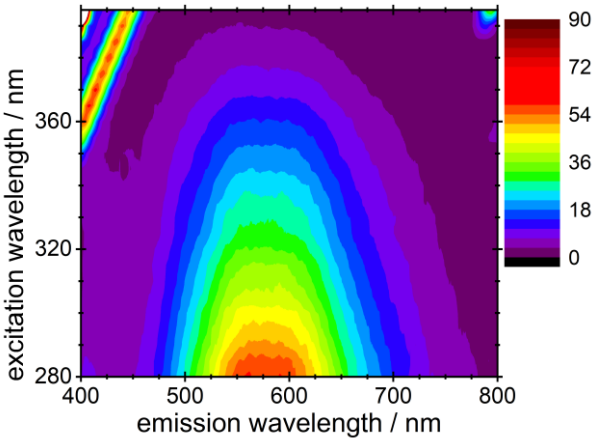

Figure S5. Static 2D luminescence excitation spectrum of **1** in EtOH with OD = 0.09 (1 cm path) at 340nm (ignore scattering artifacts in upper left/right part).

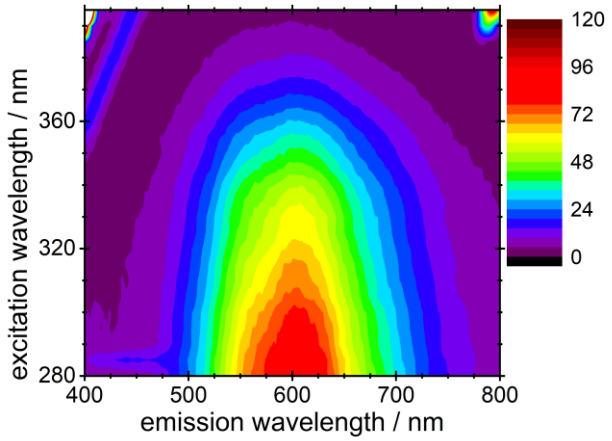

Figure S6. Static 2D luminescence excitation spectrum of **1** in DCM with OD = 0.13 (1 cm path) at 340 nm (ignore scattering artifacts in upper left/right part).

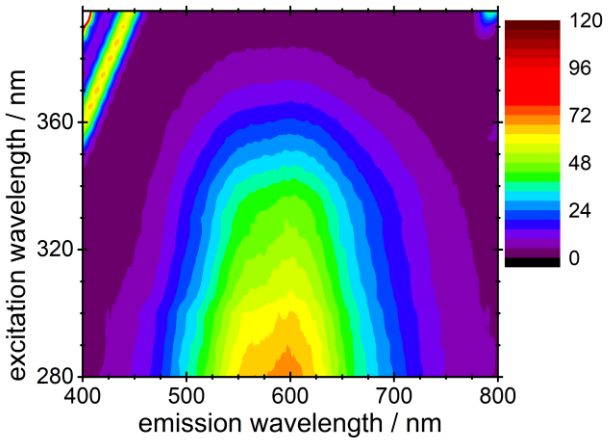

Figure S7. Static 2D luminescence excitation spectrum of **1** in THF with OD = 0.16 (1 cm path) at 340 nm (ignore scattering artifacts in upper left/right part).

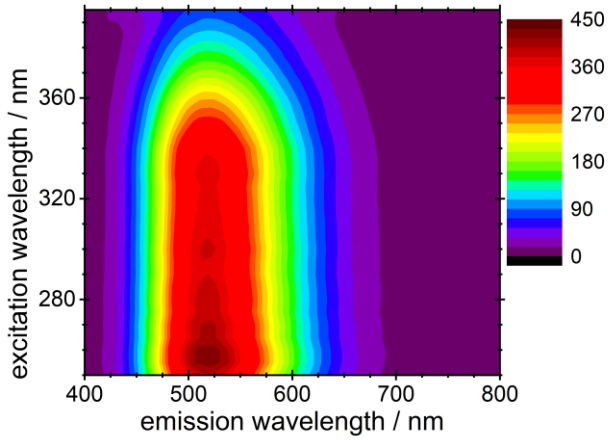

Figure S8. Static 2D luminescence excitation spectrum of **1** as neat film with OD = 0.59 at 340 nm.

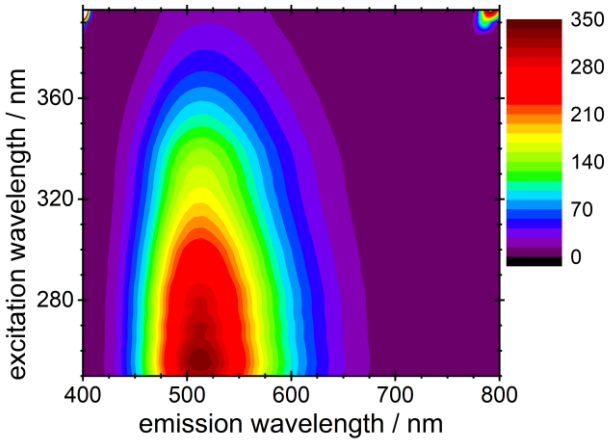

Figure S9. Static 2D luminescence excitation spectrum of **1** embedded in a PMMA matrix with OD = 0.19 at 340 nm (ignore scattering artifacts in upper left/right part).

Time resolved spectra:

UV/Vis transient absorption difference spectra, decay associated spectra and absorbance transients of 1 in THF, ACN, EtOH, DMSO and as PMMA film.

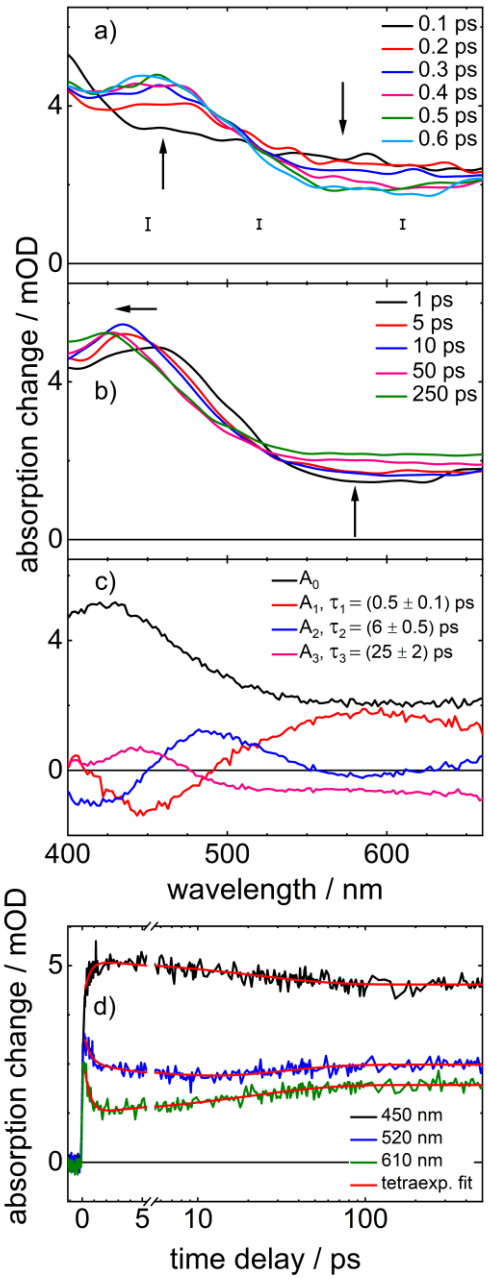

Figure S10: UV/Vis transient absorption of **1** in THF. a) sub-ps difference spectra; b) 1-250 ps difference spectra; c) DAS. Error bars for a) and b) are depicted in a) for selected wavelengths (450 nm, 520 nm, 610 nm). Data in a) and b) are smoothed *via* 10 point FFT-filter. Arrows indicate evolution of absorbance strength. d) absorbance transients for selected wavelengths (450 nm, 520 nm, 610 nm) up to 500 ps, for t > 5.5 ps logarithmic scale.

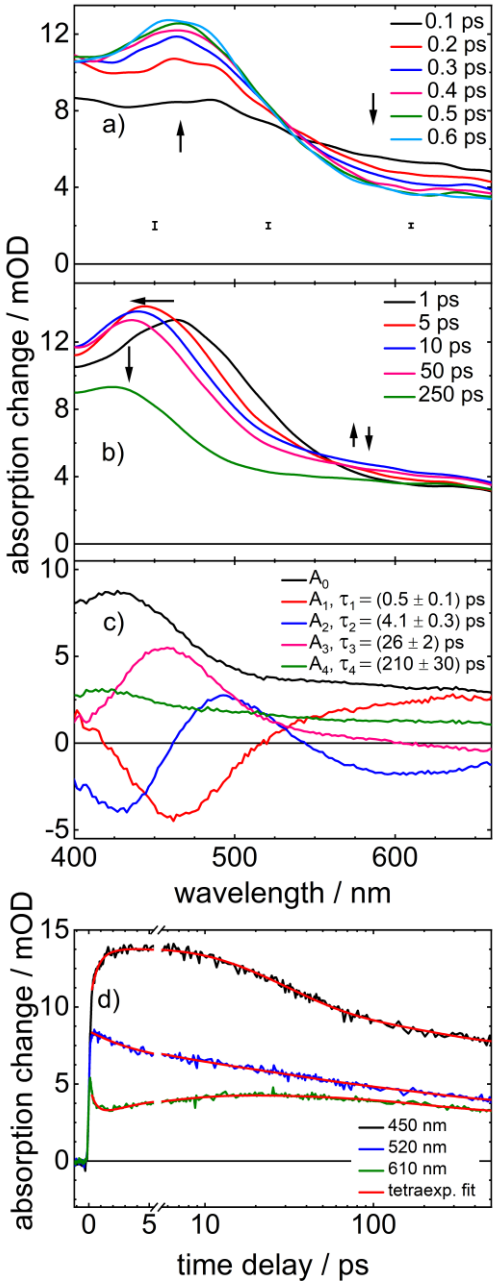

Figure S11: UV/Vis transient absorption of **1** in ACN. a) sub-ps difference spectra; b) 1-250 ps difference spectra; c) DAS. Error bars for a) and b) are depicted in a) for selected wavelengths (450 nm, 520 nm, 610 nm). Data in a) and b) are smoothed *via* 10 point FFT-filter. Arrows indicate evolution of absorbance strength. d) absorbance transients for selected wavelengths (450 nm, 520 nm, 610 nm) up to 500 ps, for t > 5.5 ps logarithmic scale.

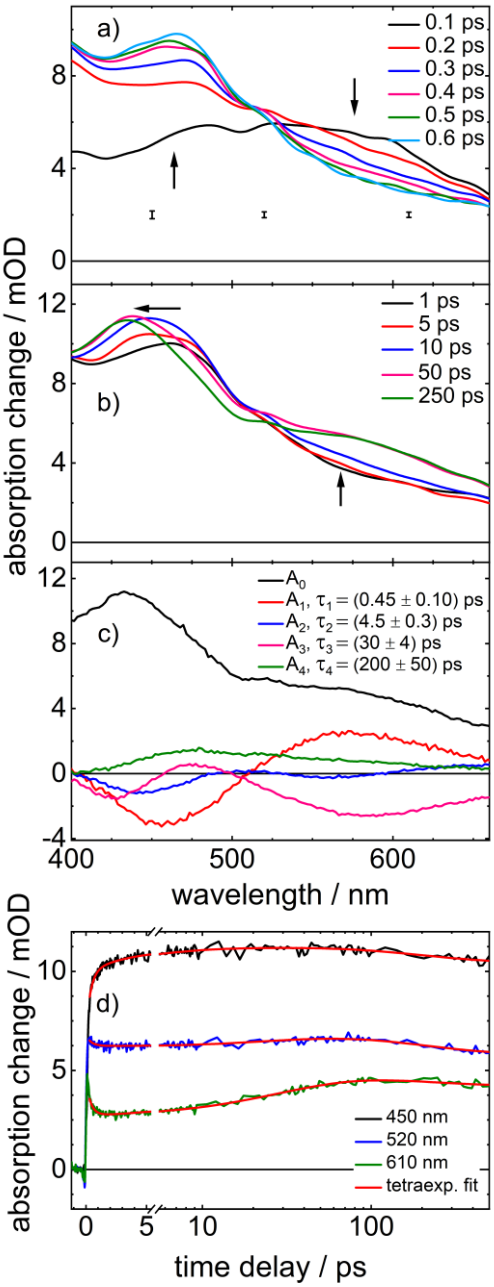

Figure S12: UV/Vis transient absorption of **1** in EtOH. a) sub-ps difference spectra; b) 1-250 ps difference spectra; c) DAS. Error bars for a) and b) are depicted in a) for selected wavelengths (450 nm, 520 nm, 610 nm). Data in a) and b) are smoothed *via* 10 point FFT-filter. Arrows indicate evolution of absorbance strength. d) absorbance transients for selected wavelengths (450 nm, 520 nm, 610 nm) up to 500 ps, for t > 5.5 ps logarithmic scale.

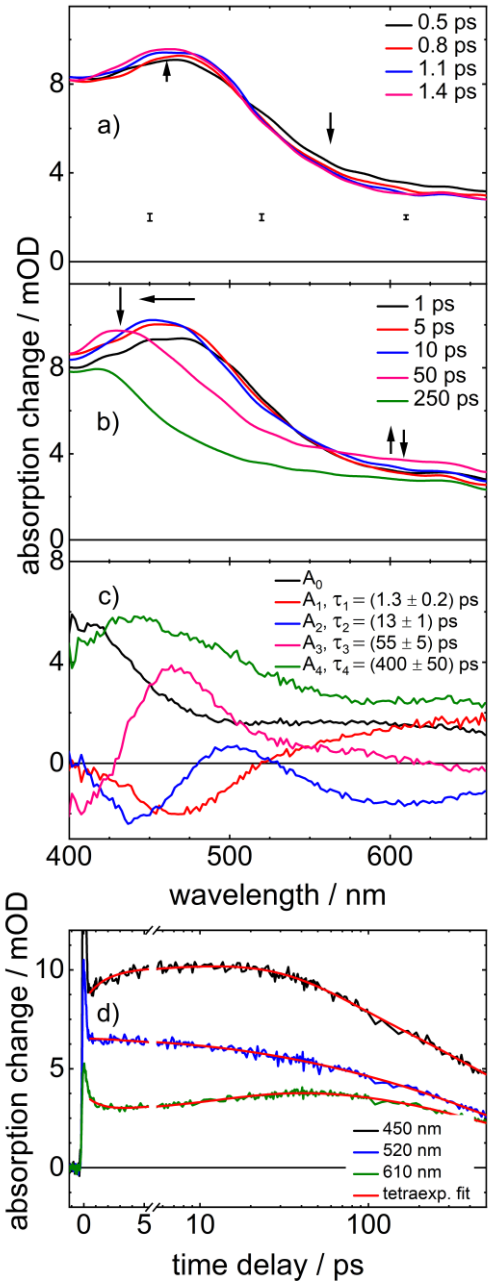

Figure S13: UV/Vis transient absorption of **1** in DMSO. a) sub-ps difference spectra (Data < 0.5 ps not shown, obscured by strong cross phase modulation); b) 1-250 ps difference spectra; c) DAS. Error bars for a) and b) are depicted in a) for selected wavelengths (450 nm, 520 nm, 610 nm). Data in a) and b) are smoothed *via* 10 point FFT-filter. Arrows indicate evolution of absorbance strength. d) absorbance transients for selected wavelengths (450 nm, 520 nm, 610 nm) up to 500 ps, for t > 5.5 ps logarithmic scale.

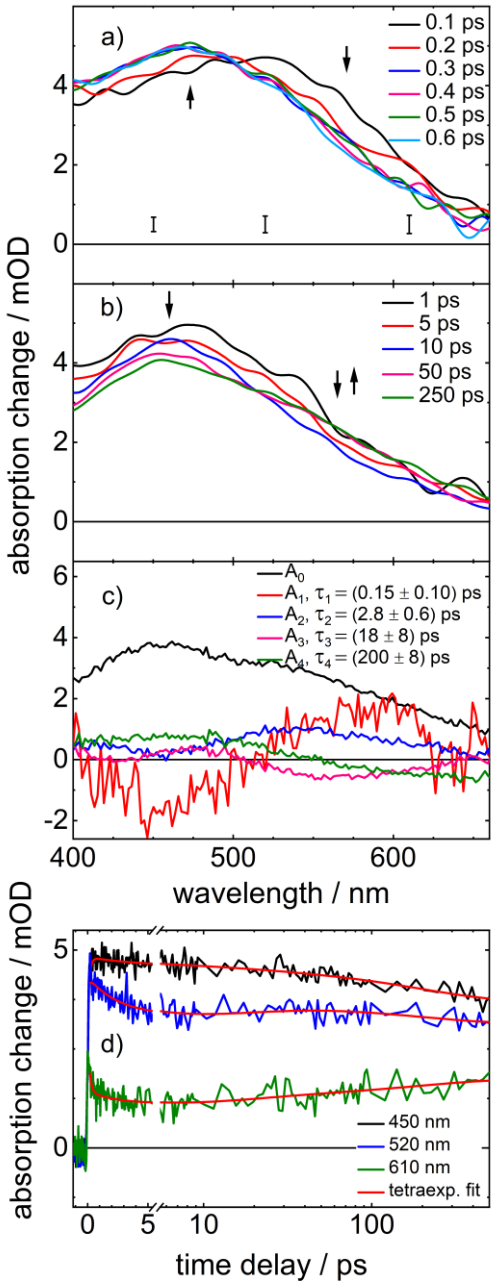

Figure S14: UV/Vis transient absorption of **1** as PMMA film. a) sub-ps difference spectra; b) 1-250 ps difference spectra; c) DAS. Error bars for a) and b) are depicted in a) for selected wavelengths (450 nm, 520 nm, 610 nm). Data in a) and b) are smoothed *via* 10 point FFT-filter. Arrows indicate evolution of absorbance strength. d) absorbance transients for selected wavelengths (450 nm, 520 nm, 610 nm) up to 500 ps, for t > 5.5 ps logarithmic scale.

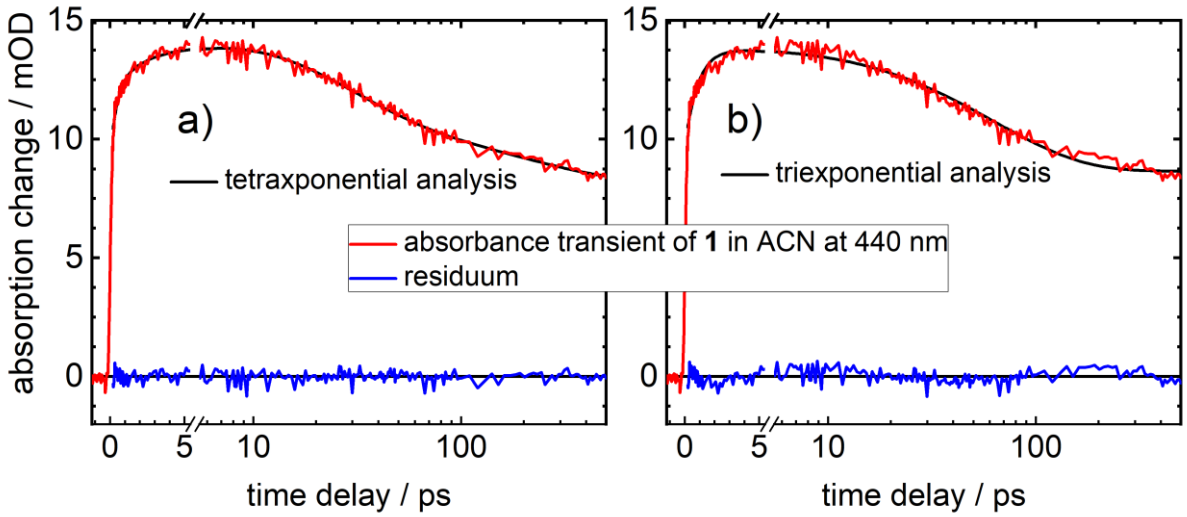

Figure S15. Absorbance transient of **1** in ACN at 440 nm, after excitation at 340 nm together with a a) tetraexponential and a b) triexponential analysis as well as the respective fit residua. Note the significantly non-zero residuum of the triexponential analysis, in particular in the time regime of τ_1 and τ_2 (below ca. 20 ps) and of τ_4 (above ca. 100 ps).

Comparison of Figure S15 a) and b) shows that an additional (forth) time constant alters the short time constants. The determination of τ_4 is probably not sufficiently accurate, however, it leads to a more precise result for shorter time scales. Note, A_4 (τ_4) could not clearly be assigned to a specific photophysical process.

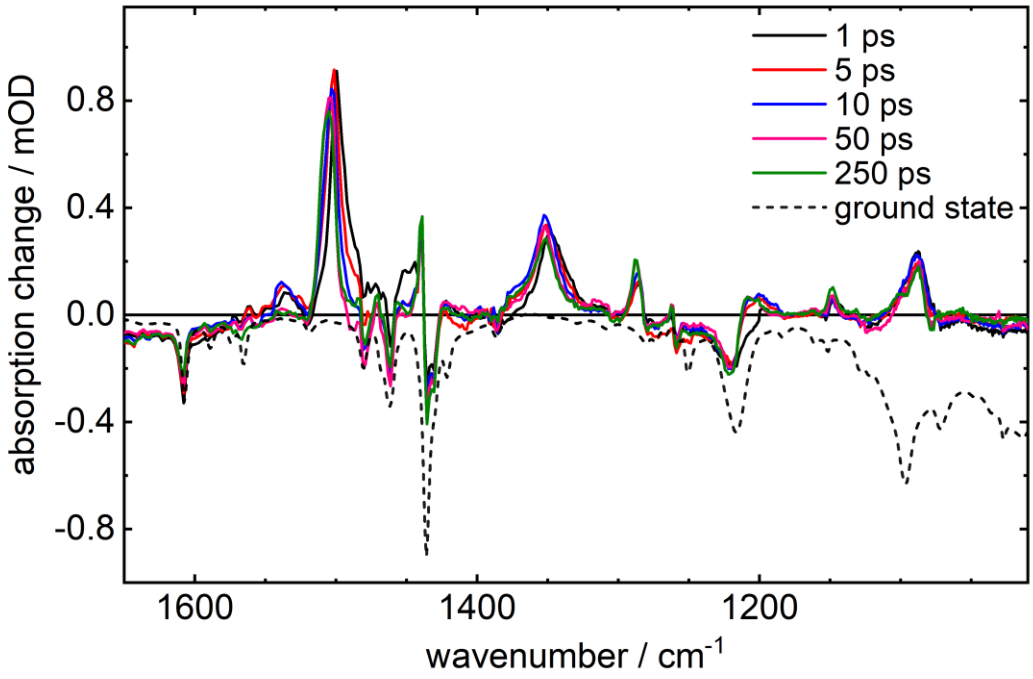

Figure S16. Overview of mid-IR difference spectra of **1** in DCM-D_2 at selected time delays. The dashed line denotes the inverted ground state spectrum.

TD-DFT (B3LYP/def2-TZVP) results:

Table S3. Assignments of selected strong and medium IR-vibrational modes of **1** (S_0, S_1, T_1) as calculated (scaled by a factor of 0.98).

Wavenumber / cm^{-1}	**Vibrational mode and electronic state**
1088	ring vib. of phenyls (S_0, S_1, T_1) and PyrTet (S_1 & T_1)
≈1160	breathing of tetrazole, ring vib. of pyridyl, H-scissoring (S_1 & T_1)
1211 & 1216	breathing vib. of tetrazole, H-scissoring and ring vib. of pyridyl (S_1 & T_1)
1227	vib. of ether bridge and ring vib. on bridged phenyls (S_0)
1243	vib. of ether bridge and ring vib. of bridged phenyls (S_1 & T_1)
1288	ring vib. and H-rocking of pyridyl, minor ring vib and H-rocking of phenyls (S_1 & T_1)
1334	ring vib and H-scissoring of pyridyl, H-rocking of phenyls (S_1 & T_1)
1370	ring vib. of tetrazole, H-rocking on pyridyl (S_1 & T_1)
1432 - 1446	H-rocking of phenyls, contributions of ring vib. of PyrTet (S_0)
1461 - 1467	H-rocking and ring vib. of O-bridged phenyls and of PyrTet (S_0, S_1, T_1)
≈1509	C-C stretch between pyridyl and tetrazole, ring vib. of PyrTet (S_1 & T_1)
1608	ring vib. of pyridyl (S_0)

Table S4. Vertical transition energies for different complex geometries (*cf.* Figure S17).

Transition	Complex geometry	Energy / cm^{-1}
$S_0 \rightarrow S_1$	S_0-geometry	28022
$S_0 \rightarrow T_1$	S_0-geometry	26034
$S_0 \leftarrow S_1$	S_1-geometry[a]	15023
$S_0 \leftarrow T_1$	T_1-geometry[b]	14204

[a] $E(S_1$ in S_0-geometry) - $E(S_1$ in S_1-geometry) = 6430 cm^{-1}
[b] $E(S_1$ in S_0-geometry) - $E(T_1$ in T_1-geometry) = 7949 cm^{-1}

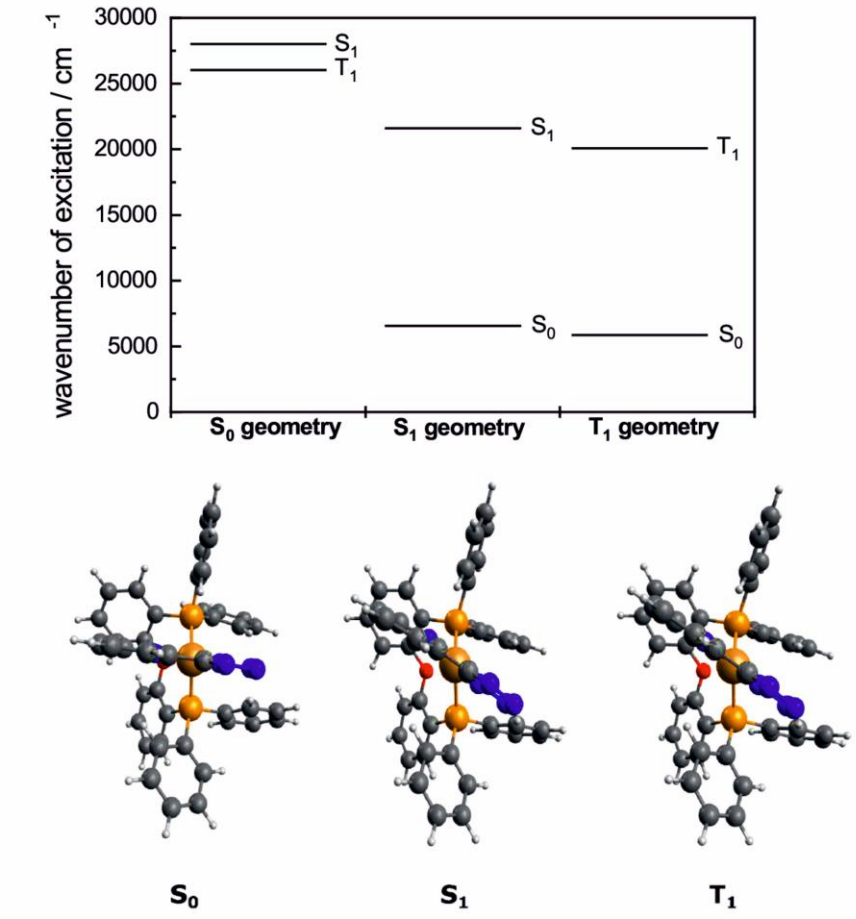

Figure S17. Calculated energies of relevant electronic states and coordination geometries of the S_0, relaxed S_1 and T_1 state. Dihedral angle between P-Cu-P- and N-Cu-N-plane for S_0: 92.5°, S_1: 51.4°, T_1: 54.5°.

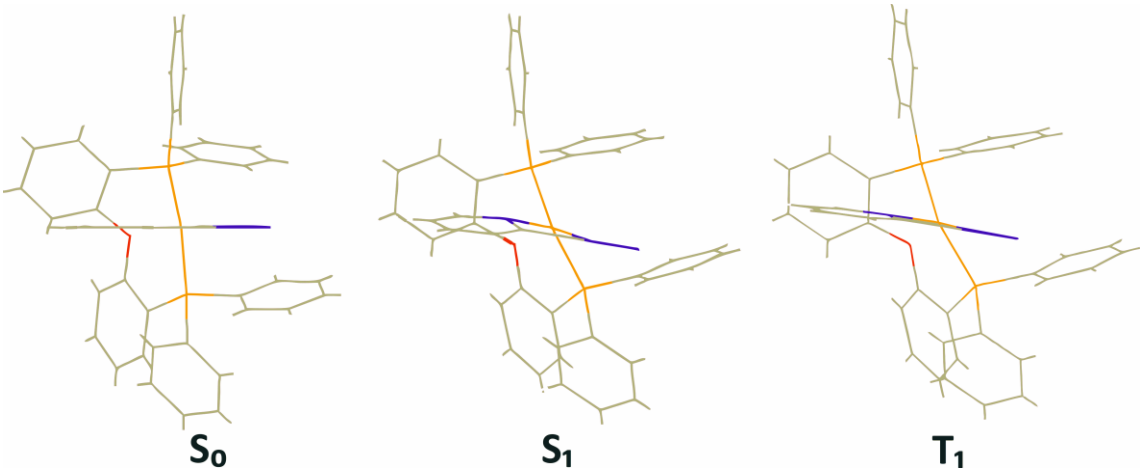

Figure S18. Calculated PyrTet ligand twist in the S_1- and T_1-state. Strongest twist is present in the S_1 state, no twist is present in the S_0 state.

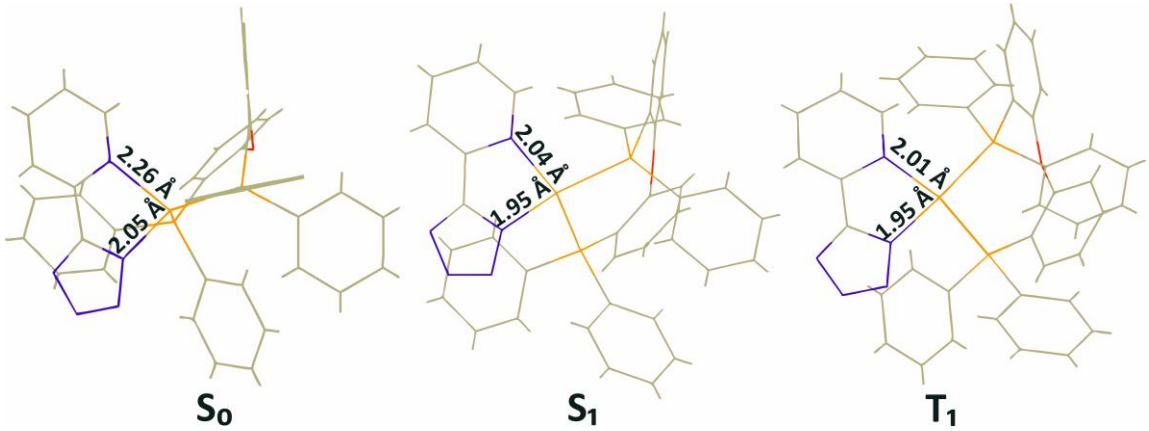

Figure S19. Structural change of the PyrTet unit along a rocking coordinate is induced by the different shortening of the respective Cu-N bonds in the relaxed S_1 state with respect to S_0. This rocking motion adds a contribution to the observed anisotropy changes $\Delta r(t)$ as described in the manuscript.

Table S5. Calculated energies of triplet states below S_1 (calculated for S_0 geometry).

Triplet state	Energy /cm^{-1}
T_5	27618
T_4	27106
T_3	26730
T_2	26581
T_1	26034

Table S6. Calculated electronic transitions with associated vertical excitation energy, oscillator strength and the orbitals (*cf.* Figure S20) contributing to the transition (with its percentage). Orbitals contributing less than 3 % are not listed. The excitation energies were scaled by a factor of 1.065 to yield best accordance with measurements (*cf.* Figure S21). This may compensate the fact that the calculations were performed in vacuum and at 0 K. The non-scaled energies are given in parentheses.

Electronic transition	**Vertical excitation energy / cm^{-1}**	**Oscillator strength**	**Orbital transition (with its percentage)**
$S_0 \longrightarrow S_1$	29843 (28022)	0.0448	193 → 195 (51.8 %) 193 → 194 (27.7 %) 192 → 195 (15.7 %)
$S_0 \longrightarrow S_2$	30065 (28230)	0.0139	193 → 194 (68.5 %) 193 → 195 (27.0 %)
$S_0 \longrightarrow S_3$	30871 (28987)	0.0236	192 → 195 (69.1 %) 193 → 195 (19.2 %) 192 → 194 (4.7 %)
$S_0 \longrightarrow S_4$	31350 (29437)	0.0111	193 → 196 (96.1 %)

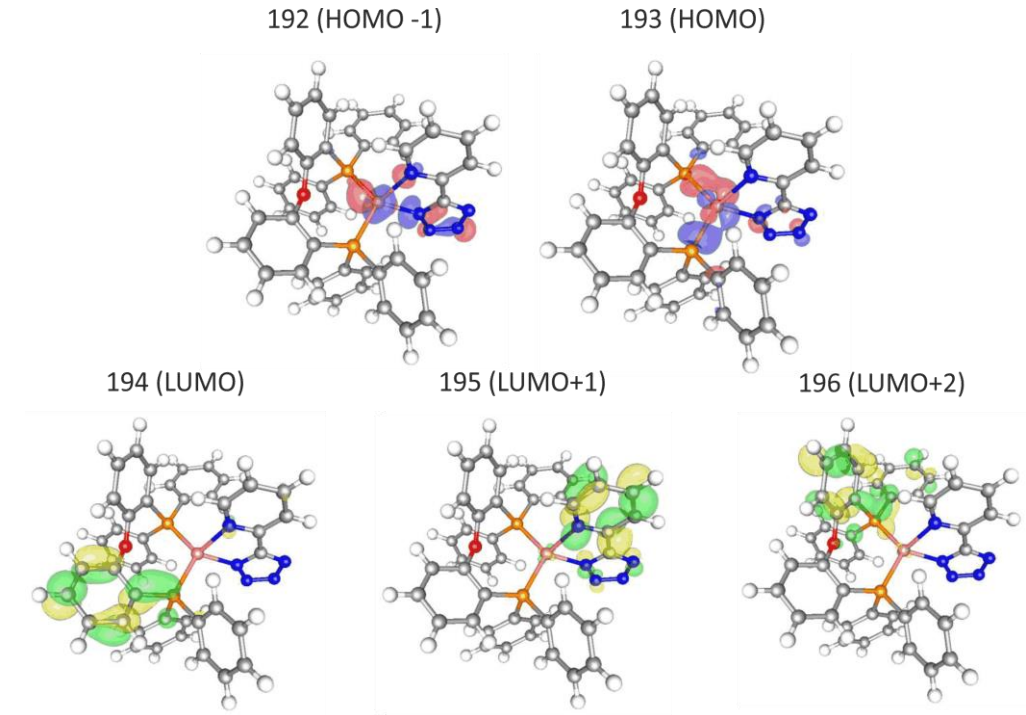

Figure S20. Images of the HOMO-1, HOMO (192, 193) and LUMO, LUMO+1, LUMO+2 (194, 195, 196) localization. For their contribution to first four singlet transitions *cf.* Table S6.

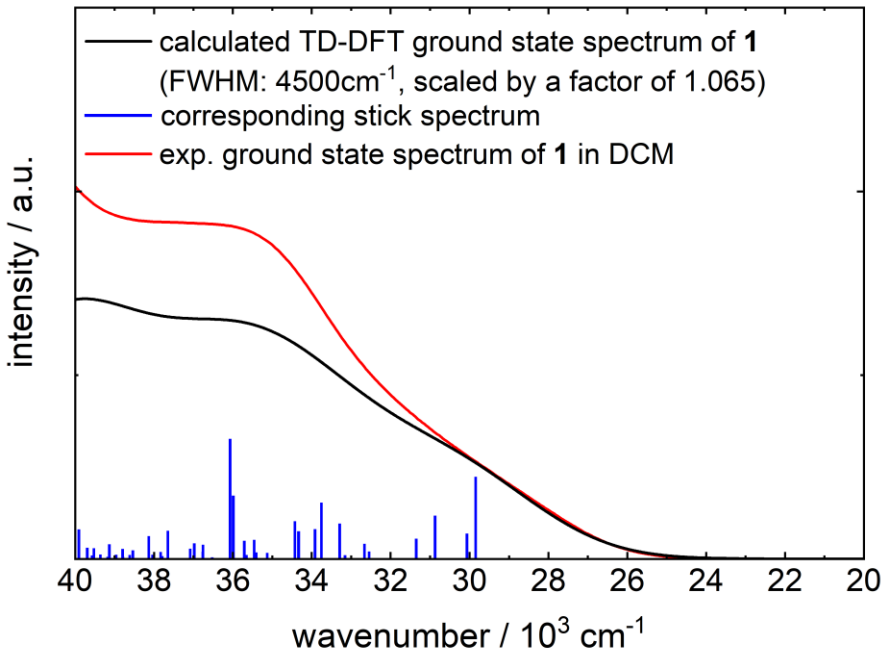

Figure S21. Comparison of the calculated and measured (in DCM) ground state absorbance spectrum of **1**. The calculated line spectrum (blue) was convolved with a Gaussian function with a FWHM of 4500 cm^{-1} (black). Calculated energies are scaled by a factor of 1.065.

The S_0 - S_1 transition is mainly dominated by transfer of electron density from the copper center (HOMO (193) and HOMO-1 (192)) to the PyrTet moiety (LUMO+1 (195)) which sums up to 67.5 %. Considering the scaled vertical transition energies (which are in good accordance with the experimental ground state spectrum of **1**, *cf.* Figure S21) and the related oscillator strength, it is most reasonable that we mainly address the S_0 - S_1 transition with our excitation wavelength of 340 nm. Possibly, we also address higher electronic transitions where the unoccupied acceptor orbital (194 and 196) is not located on the PyrTet ligand (S_0 - S_2, S_0 - S_4), however, the oscillator strengths for those transitions are comparably small (three to four times smaller compared to the S_0 - S_1 transition) with respect to electronic transitions which mainly address the acceptor orbital (195) on the PyrTet Ligand (S_0 - S_1, S_0 - S_3). Thus, the favoured and probably most significantly addressed MLCT mainly transfers electron density from the copper center on the PyrTet ligand.

Sample Integrity

Much care was taken to make sure that during measurements no significant dissociation of **1** with release of free ligands or the formation of $[Cu(PyrTet)_2]$ occurred. To rule out any influence of possible free ligands on the fs-TA data we have measured the extinction coefficient $\varepsilon(\lambda)$ for PyrTet and DPEPhos in DCM. The (small) extinction coefficient of PyrTet and DPEPhos (at the excitation wavelength of 340 nm) as compared to **1** is shown in Figure S22. Further, we have checked the static UV/Vis spectrum of **1** before and after a fs-TA measurement under realistic conditions. The neglectable degree of sample degradation is demonstrated in Figure 23. Only minor changes are discernible. Note that the absorbance of **1** at 340 nm essentially includes no contributions from

the free ligands (*cf.* Figure S22). Note as well, that in cases of observed sample degradation ($\Delta A_{340} < 10$ %), we have exchanged the sample accordingly.
Further, we have employed luminescence excitation spectra, taken from samples of **1** in DCM for fs-TA before and after measurement under realistic conditions (*cf.* Figure S24), as a sensitive mean to check for dissociation of **1** or the conceivable formation of $[Cu(PyrTet)_2]$.[1] The luminescence of the free ligands (*cf.* Figure S25 and S26) and of $[Cu(PyrTet)_2]$ (Figure S27) is not discernable in that of **1** (after fs-TA, *cf.* Figure S24). The luminescence spectra of DPEPhos were recorded in all used solvents. For the free PyrTet and $[Cu(PyrTet)_2]$ we have used only DCM, due to their very low solubility in all used solvents. The electronic ground state absorption spectrum of $[Cu(PyrTet)_2]$ is shown in Figure S28 (Note that the relatively large offset is owed to scattering by undissolved sample with low solubility of < 0.018 mmol L^{-1}). For the recording of the luminescence excitation spectra excitation only above 275 nm was used, otherwise slight sample degradation was observed.

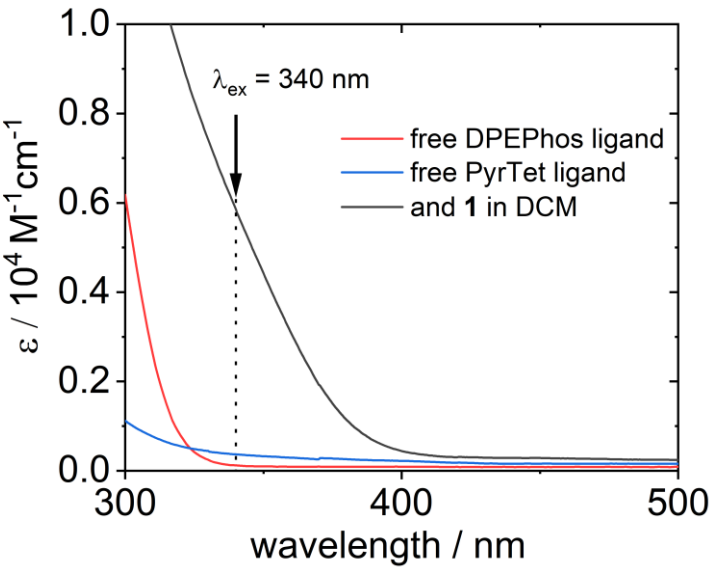

Figure S22: Extinction coefficient $\varepsilon(\lambda)$ for DPEPhos, PyrTet and **1** in DCM for comparison.

[1]Synthesis according to Zhang et al., Acta Cryst. 2006, E62, m2908–m2909; Qiu et al., Acta Cryst. 2007, E63, m2894 by J. Busch, S. Bräse (KIT Karlsruhe, Germany): Gloves, safety specs and a lab coat to be worn throughout. The PyrTet ligand (0.200 g, 1.36 mmol, 2.00 eq.), K_2CO_3 (0.282 g, 2.04 mmol, 3.00 eq.) and the colorless $CuSO_4$ (0.108 g, 0.680 mmol, 1.00 eq.) were dissolved in 15 mL DCM (SPS). The suspension turned slightly blue and was heated to 90 °C for 15 h. The color of the suspension turned even more intense pale blue solution. The pale blue suspension was added on 100 mL DCM. 200 mL of distilled water were added. The blue solid went into the water layer. The DCM phase was separated and 200 mL EE were added to the water phase. The solid was also not soluble in EE. The EE phase was separated and the water phase was filtered off and was washed with water (100 mL total), acetone (60 mL), DCM (10 mL). The compound was slightly soluble in actone and DCM. The pale blue powder was dried in vacuo. 0.159 g (0.446 mmol, 66 %) of the pale blue powder were obtained.

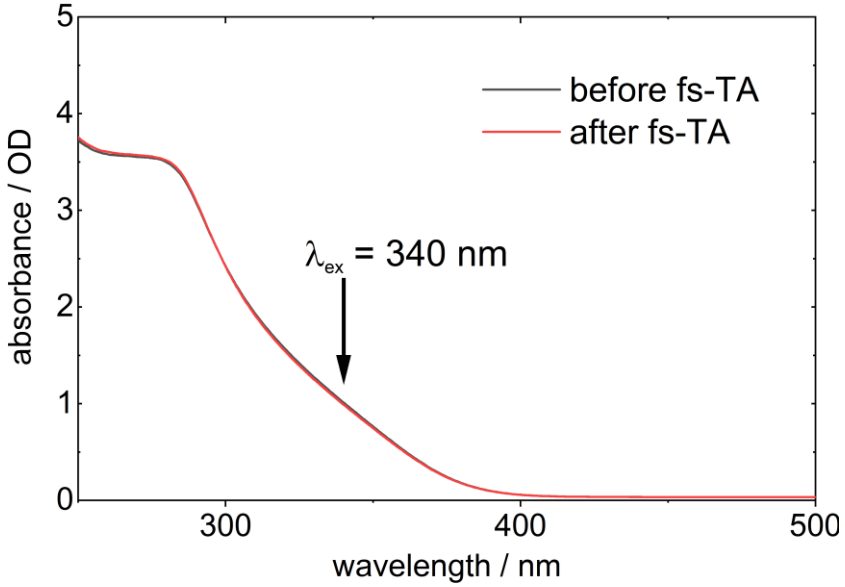

Figure S23: Absorption spectra of **1**/DCM samples used for fs-TA before and after measurement under realistic conditions.

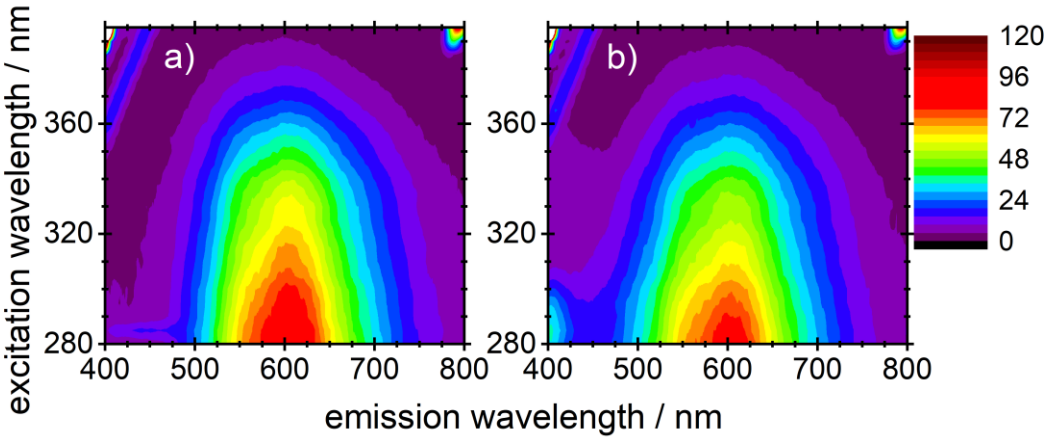

Figure S24: Luminescence excitation spectrum of **1** in DCM a) before and b) after a fs-TA measurement under realistic conditions (c = 0.02 mmol L^{-1}, respectively, ignore scattering artifacts in upper left part).

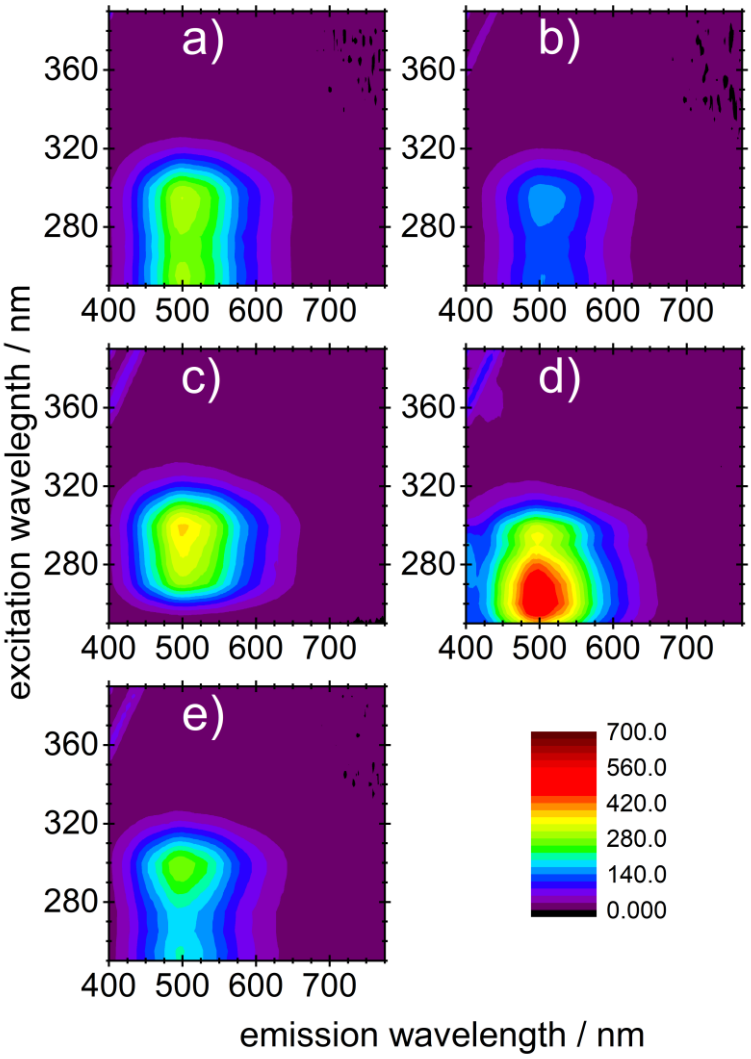

Figure S25: Luminescence excitation spectra of the free DPEPhos ligand in a) DCM (c = 0.058 mmol L^{-1}) b) ACN (c = 0.048 mmol L^{-1}) c) DMSO (c = 0.84 mmol L^{-1}) d) THF (c = 0.093 mmol L^{-1}) and e) EtOH (c = 0.093 mmol L^{-1}). For all used solvents the emission maximum is at ca. 500 nm (ignore scattering artifacts in upper left part).

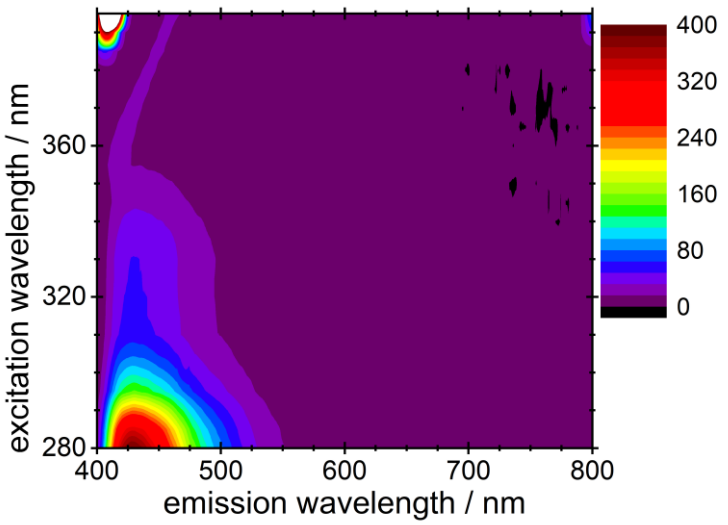

Figure S26: Luminescence excitation spectra of the free PyrTet ligand in DCM (c = 0.017 mmol L^{-1}). The emission maximum is at ca. 430 nm (ignore scattering artifacts in upper left/right part).

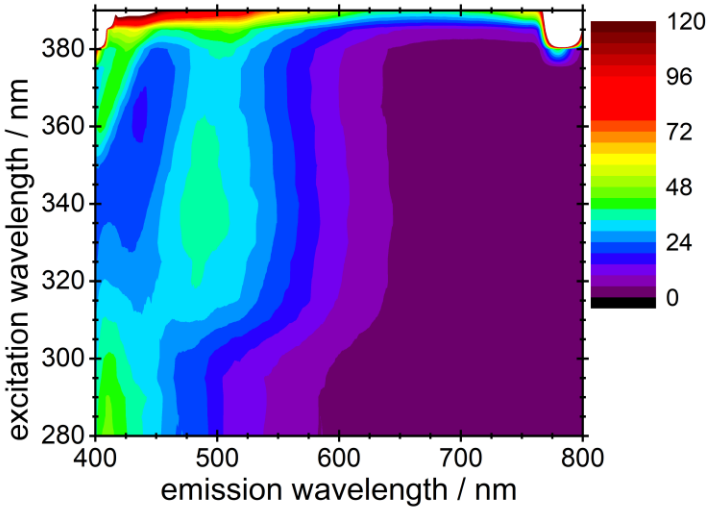

Figure S27: Luminescence excitation spectrum of $[Cu(PyrTet)_2]$ in DCM. (c << 0.018 mmol L^{-1}, very dilute solution, ignore scattering artifacts in upper left/right part).

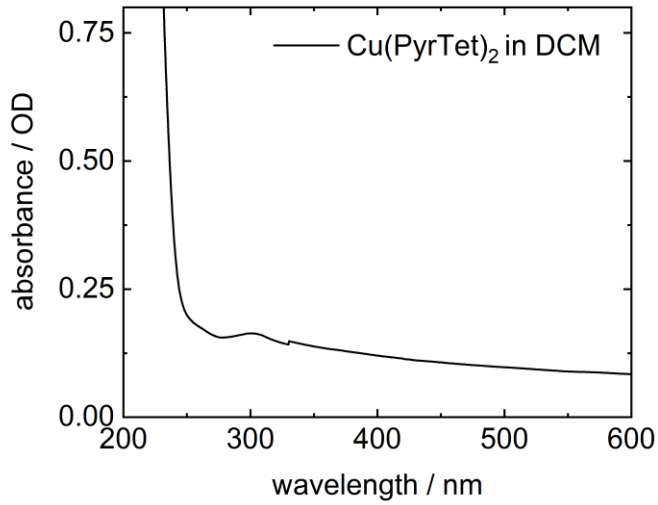

Figure S28: Electronic ground state absorption spectrum of [$Cu(PyrTet)_2$] in DCM. c < 0.018 mmol L^{-1}, not completely dissolved.

REFERENCES

1 D. R. Lide, *CRC handbook of chemistry and physics, 88th edition*, CRC press, 2007.